NASA Technical Memorandum 78950

(NASA-TM-78950) PRESSURELESS SINTERED BETA PRIME-Si3N4 SOLID SOLUTION: FABRICATION, MICROSTRUCTURE, AND STRENGTH (NASA) 19 p HC A02/MF A01 CSCL 11B

N78-29245

Unclas
G3/27 27214

PRESSURELESS SINTERED β'-Si_3N_4 SOLID SOLUTION: FABRICATION, MICROSTRUCTURE, AND STRENGTH

Sunil Dutta
Lewis Research Center
Cleveland, Ohio

TECHNICAL PAPER presented at the
Fall Meeting of the Basic Science Division
of the American Ceramic Society
Hyannis, Massachusetts, September 25-28, 1977

PRESSURELESS SINTERED β'-Si_3N_4 SOLID SOLUTION: FABRICATION, MICROSTRUCTURE, AND STRENGTH

by Sunil Dutta

National Aeronautics and Space Administration
Lewis Research Center
Cleveland, Ohio 44135

E-9731

SUMMARY

Pressureless sintering of β'-Si_3N_4 solid solution was studied as a function of temperature using Si_3N_4, AlN, and Al_2O_3 as basic constituents. Y_2O_3-SiO_2 additions were used to promote liquid-phase sintering. The sintered specimens were characterized with respect to density, microstructure, strength, oxidation, and thermal shock resistance. Density greater than 98 percent of theoretical was achieved by pressureless sintering at 1750° C. The microstructure consisted essentially of fine-grained β'-Si_3N_4 solid solution as the major phase. Modulus of rupture strengths up to 483 MPa were achieved at moderate temperature (1000° C), but decreased to 228 MPa at 1380° C. This substantial strength loss was attributed to a "glassy" grain boundary phase formed during cooling from the sintering temperature. The best oxidation resistance was exhibited by a composition containing 3 mol % Y_2O_3-SiO_2 additives. Water quench thermal shock resistance was equivalent to that of reaction sintered silicon nitride but lower than hot-pressed silicon nitride.

While work in pressureless sintering is still in the early stages, the results of strength, oxidation, and thermal shock tests are extremely encouraging and suggest that with further development, it will be possible by pressureless sintering to produce dense, high strength β'-Si_3N_4 solid solution bodies for high-temperature structural applications.

INTRODUCTION

The existence of β'-Si_3N_4 solid solution in the system Si_3N_4-Al_2O_3 was first reported by Oyama and Kamigaito[1] in Japan and by Jack and Wilson[2] in England. Subsequent studies[3,4] found that Si_3N_4-Al_2O_3 mixtures do not form a single phase β'-Si_3N_4 solid solution for any composition. Instead, β'-Si_3N_4 forms along the join Si_3N_4 and AlN-Al_2O_3 in the system Si_3N_4-AlN-Al_2O_3-SiO_2 with a metal: nonmetal ratio of 3/4.[3] The extent of the β'-Si_3N_4 solid solution is indicated in the behavior diagram as shown in Fig. 1.[5] The solid solution can be described by the formula $Si_{6-x}Al_xO_xN_{8-x}$, where $x = 0 - 4.2$.

Considerable work[6-11] on stoichiometry, structure, and properties of hot pressed β'-Si_3N_4 solid solution has been reported in the literature indicating that these ceramics have a combination of mechanical, thermal, and chemical properties, which might make them candidates for high-temperature structural applications in heat engines. These refractory ceramics are difficult to densify without hot pressing. However, hot pressing is a batch process and has limited shape capability. Therefore, it is usually not considered to be a cost effective process. As a result, effort is now being concentrated on the development of pressureless sintering methods to density these ceramics. Recently, Lumby et al.[12] reported on the fabrication and properties of β'-Si_3N_4 solid solution but the compositions and additives were not reported. Wills[13] produced high density reaction sintered β'-Si_3N_4 solid solution of composition 50 mol % Si_3N_4-25 mol % AlN-25 mol % Al_2O_3. In order to obtain high final density by pressureless sintering, additives are commonly used to promote sintering. However, the additives also limit the high-temperature strength by forming a viscous grain boundary phase.

The purpose of this study was to develop high density β'-Si_3N_4 solid solutions by pressureless sintering utilizing two levels of additive, and to determine high-temperature mechanical strength, thermal shock, and oxidation resistance.

EXPERIMENTAL PROCEDURES

The compositions investigated correspond more or less to 20 Al:80 Si/10 O:90 N (equivalent percent), as marked in the behavior diagram[5] shown in Fig. 1. "X" phase has a detrimental effect on high-temperature strength, therefore, the target composition was selected purposely below the β'-Si_3N_4 solid solution homogeneity line (Fig. 1) to prevent its formation during sintering by a shift in composition over the β'-Si_3N_4 solid solution line. The composition shift was anticipated to be very likely because of the presence of oxygen in the form of SiO_2 in the starting materials, and further utilization of oxide additives. The basic constituents were Si_3N_4, AlN, and Al_2O_3. To them were added minor amounts of additives Y_2O_3-SiO_2, to promote sintering. A molar ratio of 1:2 was chosen to form $Y_2Si_2O_7$ phase, which has been found to be compatible with β'-Si_3N_4 solid solution, according to the phase diagram[14] shown in Fig. 2. Further, it was anticipated that the $Y_2Si_2O_7$ phase might improve the oxidation behavior since both Y_2O_3 and SiO_2 are in the highest state of oxidation, thus acting as a barrier for further diffusion of oxygen in the sintered material. Using the target composition 20 Al:80 Si/10 O:90 N (equivalent percent), two different mixtures were made with Si_3N_4, AlN, Al_2O_3, Y_2O_3, and SiO_2 powders with two levels in the Y_2O_3-SiO_2 additive system. For simplicity, they are to be referred as composition A and B containing 6 mol % and 3 mol % Y_2O_3-SiO_2. These are listed in Table I. The Y_2O_3 to SiO_2 molar ratio was always constant at 1:2. The purpose of utilizing the additive system (Y_2O_3-SiO_2) was to develop a process capable of yielding fully dense β'-Si_3N_4 solid solution by pressureless sintering under a nitrogen pressure of 1 atmosphere.

Commercial grade Si_3N_4, AlN, Al_2O_3, Y_2O_3, and SiO_2 powders were used in the fabrication studies. Mixtures for 100 gram batches were wet milled in polyethylene bottles for 17 to 20 hours using high alumina grinding media and ethanol. The starting compositions were adjusted to allow for pick up of alumina from the mills. The pick up varied slightly depending on the milling time and weight of the ball charge but was typically 0.8 wt % for a 200 gram ball charge (in a 100-g powder charge) milled for 17 to 20 hours.

After milling, the slurry was dried on a heated aluminum plate, and sieved through a 60-mesh sieve to break up the agglomerates. Twenty grams of mixed powder was cold formed into rectangular blocks of 7.6 by 2.5 by 0.64 cm, by die pressing followed by cold isostatic pressing of four blocks in one batch (in rubber bags) at a total pressure of 414 MN/m^2.

The compacts were pressureless sintered in a "cold-wall" furnace at temperatures between 1450° and 1750° C for periods of 1 to 2 hours under nitrogen pressure of 1 atmosphere. After sintering, the compacts were furnace cooled.

Sintered specimens were machined into test bars and the surfaces were subsequently ground with a 220-grit diamond wheel to a final surface roughness of 10 to 15 microinches rms. The final dimensions of the test bars were 2.54 by 0.64 by 0.32 cm with four edges beveled.

Density was measured on the machined test bars by liquid immersion and pycnometric methods. Microstructural characterization was made by optical microscopy and transmission electron microscopy, while phase identification and elemental analysis were carried out by X-ray diffraction and EDAX techniques.

Modulus of rupture tests were conducted by four point loading with 0.95 cm top and 1.87 cm bottom spans. Testing was done at room temperature, 1000°, 1200°, and 1380° C. All testing was conducted in air with a cross head velocity of 0.02 cm/min. Fracture surfaces of selected test specimens were examined in the scanning electron microscope to determine the fracture origins

For oxidation tests, the machined bars (2.54 by 0.64 by 0.32 cm) were placed in a platinum crucible. The crucible was introduced into a preheated furnace and automatically cycled. Each cycle consisted of 1 hour at 1375° C followed by 20 minutes cooling. After each 15 hours at temperature (20 hr elapsed time) had accumulated, the bars were separately weighed. The cyclic heating was continued for a total of 90 hours at temperature. Characterization of the oxide scales was performed by light microscopy and X-ray diffraction.

Thermal shock tests were conducted by holding the bars in a vertical tube furnace for 15 minutes to reach an equilibrium temperature and dropping them into a container of water at room temperature. The severity of thermal shock was adjusted by varying the temperature of the tube furnace. Strength after thermal shock was measured at room temperature in a four point bend test with a cross head speed of 0.02 cm/min.

RESULTS AND DISCUSSIONS

A. Powder Characterization

Impurity analyses of the "as-received" powders are shown in Table II, indicating that the AlN starting powder contained most of the major impurities found, that is, Fe, Si, Ti, W, Ni, while the starting powder Y_2O_3 had only Al as a major impurity. All other powders Si_3N_4, Al_2O_3, and SiO_2 were relatively free from such impurities. The oxygen content of the starting Si_3N_4 powder was 2.7 wt %, while the specific surface area (BET method) was 11.84 m^2/g The surface areas of other starting powders were 3.40 m^2/g for AlN; 14.45 m^2/g for Al_2O_3; 5.16 m^2/g for Y_2O_3; and 158.46 m^2/g for SiO_2.

B. Densification

Densification behavior of compositions A and B as a function of temperature is shown in Fig. 3. Very rapid densification takes place between 1550^o and 1650^o C. At 1700^o C, maximum density of 3.08 g/cc was obtained in the composition A with 6 mol % Y_2O_3-SiO_2 additives, while with 3 mol % additives in composition B, the density was 2.94 g/cc. These values are approximately 98 percent of theoretical for composition A and 94 percent of theoretical for composition B, on the basis of an assumed density of 3.14 g/cc for the blend of Si_3N_4, AlN, and Al_2O_3,[15] adjusted for the additions of Y_2O_3 and SiO_2. Densification was facilitated by increased Y_2O_3-SiO_2 additives. Further, the densification of these mixtures is consistent with a liquid phase sintering process,[11, 16] and appears to be analogous to that of silicon nitride.[17-20]

C. Characterization

X-ray diffraction examinations were made for phase identification in the sintered specimens. Figure 4 shows X-ray diffraction results of compositions A and B sintered at 1700^o C for 1 hour. The diffraction pattern for both compositions were almost identical in every detail, and only β'-Si_3N_4 solid solution was detected as a major phase. No other phases or additional peaks of significant intensities were observed. Also, no $Y_2Si_2O_7$ could be detected in either of the sintered compositions. This observation is consistent with those of Rowcliffe et al.[19] and Smith,[20] who also did not find the crystalline $Y_2Si_2O_7$ phase in sintered Si_3N_4 specimens utilizing Y_2O_3 sintering aid. It is concluded that the additives Y_2O_3-SiO_2 most probably formed an yttria-silica glassy phase, which became liquid at the sintering temperature and thus facilitated densification. The presence of such a noncrystalline phase although not identifiable by X-rays was deduced either from the observed deterioration of mechanical properties[21] at elevated temperatures or from the observation of presumed devitrification products after heat treatment.[22]

Microstructure characterization was made by optical microscope, transmission microscope and energy dispersive X-ray analysis (EDAX) techniques. Figure 5 shows typical microstructures developed in the sintered compositions A and B. The microstructures consist of an essentially single phase β'-Si_3N_4 solid solution (light gray) phase with isolated porosity (dark gray) combined with some pull outs from polishing.

The porosity was typically associated with the lower density of the sintered specimens from composition B. Several "white" particles were also identified in very limited areas and were examined in the SEM using X-ray energy dispersive spectrometer. Spectra were taken from several of these particles and the matrix. Si and Al were detected only in the matrix. Elements detected in the white metallic particles were Fe, W, Ti, Cr, and Mo, which can be attributed to the impurities present in the "as-received" AlN powder as indicated in Table II.

Further microstructural characterization was conducted on electron transparent specimens. Figures 6 and 7 show typical transmission micrographs of sintered material. Composition A with 6 mol % Y_2O_3-SiO_2 additives had a mixture of equiaxed grains ranging between 0.15 to 1.2 μm, and columnar grains of size range 0.15 μm wide by 2.0 μm long to 1.3 μm wide by 5.0 μm long (Fig 6). By contrast, composition B containing 3 mol % additives had predominantly equiaxed grains of size range 0.25 to 2.0 μm (Fig. 7). Indications of a noncrystalline phase, which however, could not be identified, were present in the microstructures at the triple grain intersections. The grain morphology, in all instances, is typical of liquid phase sintering and solution reprecipitation mechanisms, that is, the silicate liquid forms the reactive transport medium in the form of a thin layer between transforming crystals. The liquid phase is retained in intercrystalline spaces, and grain boundaries, during cooling from the sintering temperature.

D. Modulus of Rupture Test

Modulus of rupture tests were conducted to evaluate the strength of the sintered β'-Si_3N_4 solid solution at both room and elevated temperatures. Machined bend bars from both compositions (A and B) having density values 3.08 and 2.94 g/cc were evaluated. The variation in M.O.R. strength as a function of temperature to 1380° C is plotted in Fig. 8. Each point on the curve is the average of four tests. Average strengths for composition A (6 mol % Y_2O_3-SiO_2) were 483 MPa up to a temperature of 1000° C 345 MPa at 1200° C and 220 MPa at 1380° C. For composition B (3 mol % Y_2O_3-SiO_2), the average M.O.R. strength was 428 MPa at room temperature, 400 MPa at 1000° C, 324 MPa at 1200° C, and 228 MPa at 1380° C. The lower strength value for composition B at room temperature can be attributed to higher porosity than that in composition A. On the other hand, the lower strength values at 1200° and 1380° C for both compositions A and B can be attributed to the effect of additives (Y_2O_3-SiO_2), which formed a grain boundary amorphous phase(s) which, in turn, became viscous at the test temperatures. This behavior is analogous to that of both sintered and hot pressed Si_3N_4 containing MgO,[21] Y_2O_3,[17,18] CeO_2,[23] ZrO_2,[23] etc. It was anticipated, however, that a lower amount of additives or liquid phase(s) might result in greater high-temperature strength in the sintered materials. However, the present results indicated that the strength values at 1380° C are almost equivalent for composition A containing 6 mol % additives as compared to composition B containing 3 mol % additives. The exact effect of the amount of additives on the high temperature strength cannot be explained in the present study due to the fact that composition B, although containing less additives, also has lower density than that of composition A, which could counterbalance any effect of additives on improvement in strength.

Fracture surfaces of selected broken bend bars were examined to identify the origin of fractures. In most cases, the room-temperature fractures appeared to initiate from surface or edge flaws, indicating that better surface preparation might lead to improved strengths. On the other hand, high-temperature fractures were due to slow crack growth regions, where the crack front advanced along the grain boundaries resulting in an intergranular failure which is typical of Si_3N_4 based ceramics. These are shown in Figs. 9 (composition A) and 10 (composition B). While Fig. 9(a) shows room-temperature brittle fracture, Figs. 9(b) and (c) are fracture surfaces at 1200^o and 1380^o C, respectively, showing the fracture initiation site (V-shaped area when the two halves joined together), which is typical of slow crack growth at high temperatures. Similar behavior was observed in the fracture surfaces of composition B, which are shown in Figs. 10(a), (b), and (c).

E. Oxidation

Oxidation tests were carried out under identical conditions for both composition A and composition B. The oxidation cycle consisted of 1 hour at temperature (1375^o C) followed by 20 minutes cooling. After each 15 hours at temperature (20 hr elapsed time) had accumulated, weight gain for each bar was measured separately. Weight gain versus time for compositions A and B is linearly plotted in Fig. 11, while the parabolic plot is in Fig. 12. Composition A with 6 mol % Y_2O_3-SiO_2 additives exhibited a higher weight gain than composition B with 3 mol % Y_2O_3-SiO_2, that is, less oxidation resistance than composition B, although it had been anticipated initially that composition A would exhibit better oxidation resistance than composition B due to its higher Y_2O_3-SiO_2 content. Both compositions A and B exhibited more or less parabolic rate behavior which is shown in Fig. 12. However, in composition A, a change in the slope of the paraboiic plot was observed after approximately 30 hours of oxidation time and parabolic behavior continued at the new slope for the duration of the test. Whether this change in parabolic behavior was due to different types of reaction[24] occurring during oxidation, for example, reaction with the impurities, phase transformation or spalling was not determined.

The oxide scale in composition A was identified by X-ray to contain cristobalite as the major phase with minor amounts of mullite, while in composition B, mullite was the major phase with minor amounts of cristobalite. Further, composition A produced thick oxide scales whitish in color with a rough surface, while composition B exhibited thin scales with smooth surface. These differences were attributed to the different nature of the oxidation products from composition B.

F. Thermal Shock

The water quench thermal shock test was performed on a total of 20 test bars of composition A only. After quenching from various temperatures into water at room temperature, the test bars were dried, and 4-point modulus of rupture strength was measured at room temperature on each thermally shocked bar to determine the residual strength. These values are plotted as a function of quenching temperature difference as shown in Fig. 13. Each point on the curve is the average of four tests. No strength loss was observed up to a temperature difference of 300° C, followed by a gradual strength loss in a "quasi-static"[25] manner up to 460° C, after which the strength drop was catastrophic.

The ΔT °C was determined to be between 460° to 480° C (Fig. 13). The value was found to be higher than that of various silicon carbide ceramics, equivalent to that of reaction sintered silicon nitride but lower than hot pressed silicon nitride[26] which are shown in Fig. 13. The result suggests that the pressureless sintered β'-Si_3N_4 solid solution possess thermal shock resistance comparable to that of materials which are currently being considered for high-temperature applications.

CONCLUDING REMARKS

The experimental studies reported here have shown that high density β'-Si_3N_4 solid solution can be prepared by pressureless sintering ultrafine Si_3N_4, AlN, and Al_2O_3 powders with an Y_2O_3-SiO_2 additive system, under relatively simple sintering conditions. Densification takes place by a liquid phase sintering mechanism involving solution of α-Si_3N_4 and reprecipitation as β'-Si_3N_4. The sintered product is essentially β'-Si_3N_4 solid solution. No crystalline $Y_2Si_2O_7$ could be detected suggesting the formation of an yttria-silica glassy phase during sintering. Strengths up to 483 MPa (70 000 psi) are achieved at moderate temperature (1000° C), while a substantial strength loss occurs at high temperature (1380° C). It is believed that this problem can be overcome by better understanding of the grain boundary recrystallization process.

The oxidation resistance of a composition containing 3 mol % Y_2O_3-SiO_2 is better than the oxidation resistance of a composition containing 6 mol % (Y_2O_3-SiO_2). In thermal shock, β'-Si_3N_4 solid solution exhibits higher resistance than silicon carbide and resistance equivalent to reaction sintered silicon nitride but lower than hot pressed silicon nitride.

The results of strength, oxidation, and thermal shock tests at this stage in our development of β'-Si_3N_4 solid solution are comparable to many currently sintered silicon nitride based ceramics and are extremely encouraging; they suggest that, with further development, it will be possible to make sintered β'-Si_3N_4 solid solution with properties suitable for high-temperature applications.

REFERENCES

1. Y. Oyama and O. Kamigaito, "Silicon Nitride-Alumina System Sintered Materials," Yogyo Kyokai Shi (Tokyo), 80 (8) 327-36 (1972).
2. K. H. Jack and W. I. Wilson, "Ceramics Based on the Si-Al-O-N and Related Systems," Nature (Phys. Sci.), 238 (80) 28-29 (1972).
3. R. J. Lumby, B. North, and A. J. Taylor; pp. 283-298 in Special Ceramics 6. Edited by P. Popper, British Ceramic Research Assn., London, 1975.
4. G. K. Layden, "Process Development for Pressureless Sintering of SiALON Ceramics Components," R75-912072-4, United Technologies Corp., January 1976.
5. K. H. Jack, "SiALONs and Related Nitrogen Ceramics," J. Mater Sci., 11 (6), 1135-1158 (1976).
6. W. J. Arrol, pp. 729-738 in Ceramics for High-Performance Applications. Edited by J. J. Burke, A. E. Gorum and R. N. Katz, Brook Hill Publishing Co., Chestnut Hill, Mass., 1974.
7. F. F. Lange and S. C. Singhae, "Fabrication and Properties of Silicon Compounds: Task I, Fabrication, Microstructure, and Selected Properties of SiALON Compositions," Westinghouse Research Labs., Pittsburgh, February 1974. (AD-786750)
8. W. B. Crandall, A. Z. Hed, and L. E. Shipley, "Preparation and Evaluation of SiALON," ARL-74-0099, IIT Research Institute, Chicago, June 1974.
9. P. Drew and M. H. Lewis, "The Microstructures of Silicon Nitride/Alumina Ceramics," J. Mater. Sci., 9 (11), 1833-38 (1974).
10. P. L. Land, J. M. Wimmer, R. W. Burns, and N. S. Chaudhury, "Compounds and Properties of the Si-Al-O-N System," J. Am. Ceram. Soc., 61 (1-2) 56-60 (1978).
11. H. C. Yeh, W. A. Sanders, and J. L. Fiyalko, "Pressure Sintering of Si_3N_4-Al_2O_3 (Sialon)," Am. Ceram. Soc. Bull., 56 (2) 189-193 (1977).

12. R. J. Lumby, B. North, and A. J. Taylor, "Engineering Properties of Sintered SiALONS, and Some Applications in Metal Handling and Cutting," Paper presented at the Newport Conference for High Performance Applications," Newport, R. I. (1977).

13. R. R. Wills, R. W. Stewart, and J. M. Wimmer, "Fabrication of Reaction Sintered SiALON," J. Am. Ceram. Soc., 60 (1-2), 64-67 (1977).

14. R. R. Wills, S. Holmquist, J. M. Wimmer, and J. A. Cunningham, " Phase Relationship in the System Si_3N_4-Y_2O_3-SiO_2," J. Mater. Sci., 11 (7) 1305-1309 (1976).

15. G. K. Layden, "Development of SiALON Materials," R75-912184-3, United Technologies Corp., September 1975.

16. M. H. Lewis, B. D. Powell, P. Drew, R. J. Lumby, B. North, and A. J. Taylor, "The Formation of Single Phase Si-Al-O-N Ceramics," J. Mater. Sci., 12 (1) 61-74 (1977).

17. G. E. Gazza, "Hot Pressed Si_3N_4," J. Am. Ceram. Soc., 56 (12) 662 (1973).

18. M. Mitomo, "Pressure Sintering of Si_3N_4," J. Mater Sci., 11 (6) 1103-1107 (1976).

19. D. J. Rowcliffe and P. J. Jorgensen, "Mechanical Properties of Sintered Si_3N_4," Paper presented at the Fall Meeting of the Basic Science Division of the American Ceramic Society, Hyannis, Mass. Sep. 25-28 (1977), Paper 57-BN-77F Abstracted in Am. Ceram. Soc. Bull. 56 (8) 734 (1977).

20. J. T. Smith, "Properties of Fully Dense, Sintered Si_3N_4 Compositions," Paper presented at the Fall Meeting of the Basic Science Division of the American Ceramic Society, Hyannis, Mass., Sep. 25-28 (1977). Paper 61-BN-77F abstracted in Am. Ceram. Soc. Bull. 56 (8) 734 (1977).

21. F. F. Lange and J. L. Iskoe, pp. 223-238 in Ceramics for High Performance Applications. Edited by J. J. Burke, A. E. Gorum, and R. N. Katz, Brook Hill Publishing Co., Chestnut Hill, MA, 1974.

22. M. E. Milberg and W. M. Miller, "Observation of a Noncrystalline Phase in Sintered Si_3N_4-Al_2O_3-Y_2O_3," submitted to the J. Amer. Ceram. Soc. (To be published).

23. G. K. Layden, "Development of SiALON Materials," R77-912184-21, United Technologies Corp., December 1977.

24. W. C. Tripp and H. C. Graham, "Oxidation of Si_3N_4 in the Range 1300 to 1500 C," J. Am. Ceram. Soc., 59 (9-10) 399-403 (1976).

25. D. P. H. Hasselman, "Unified Theory of Thermal Shock Fracture Initiation and Crack Propagation in Brittle Ceramics," J. Am. Ceram. Soc., 52 (11) 600-604 (1969).

26. C. C. Seaton, "Thermal and Acoustic Fatigue of Ceramics and Their Evaluation," AMMRC MS 74-7, Army Materials and Mechanics Research Center, Watertown, MA, June 1974. (AD-785547)

TABLE I. - MATERIAL COMPOSITIONS

FOR β'-Si_3N_4 SOLID SOLUTION

Material	Mol %		Wt %	
	A	B	A	B
Si_3N_4	52	54	71	73.5
AlN	32	33	13	13.1
Al_2O_3	10	10	10	10
Y_2O_3	2	1	4	2.2
SiO_2	4	2	2	1.2

TABLE II. - TRACE IMPURITY ANALYSIS OF

RAW POWDERS (ppm)

Element	Si_3N_4 GTE	AlN Shield alloy	Al_2O_3 Linde A	SiO_2 Apache	Y_2O_3 United Mineral
Al	--	Major	Major	100	640
Co	50	110	---	---	---
Cu	--	100	---	70	---
Cr	--	210	---	50	90
Fe	70	1750	70	180	160
Mg	--	----	110	110	90
Mn	--	120	---	---	---
Mo	--	290	---	---	---
Ni	--	130	---	---	---
Si	Major	400	154	Major	230
Ti	--	390	---	---	---
V	--	140	---	---	---
W	--	470	---	---	---
Zr	--	160	---	---	---

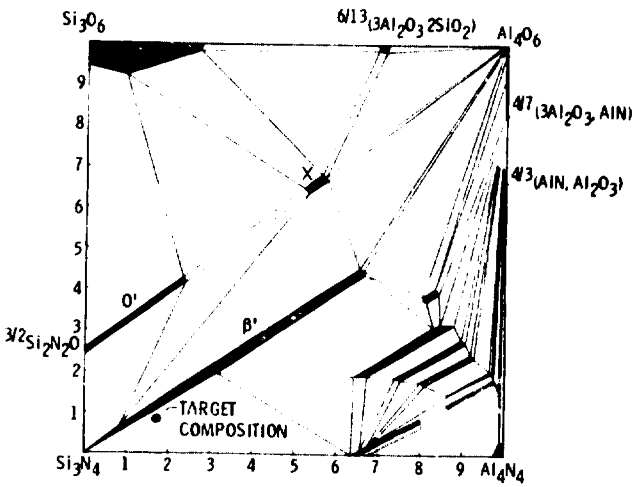

Figure 1. - The Si_3N_4-AlN-Al_2O_3-SiO_2 system (after Jack[5]).

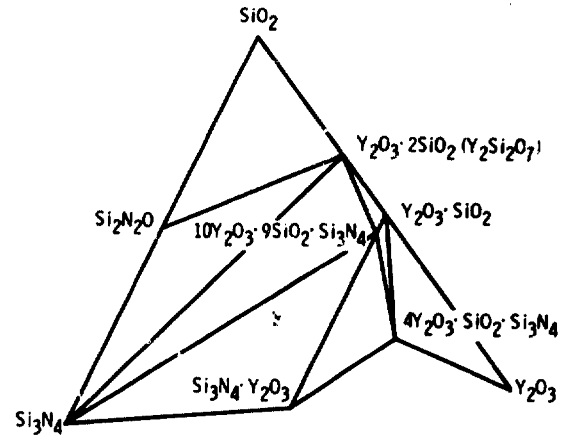

Figure 2. - The system Si_3N_4 - Y_2O_3 - SiO_2 showing solid-solid equilibria at 1700 (after Wills[14]).

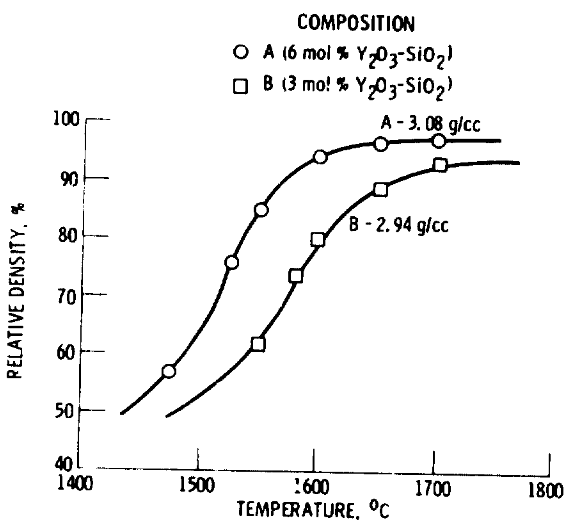

Figure 3. - Density of β'-Si_3N_4 solid solutions for 1 hour at different temperatures.

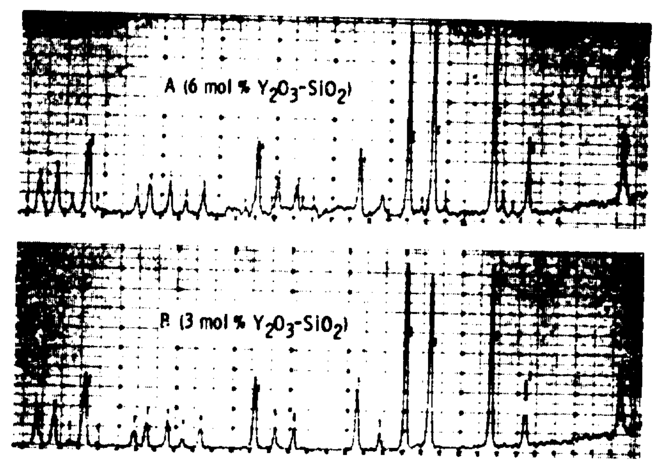

Figure 4. - X-ray diffraction data of β'-Si_3N_4 solid solution compositions.

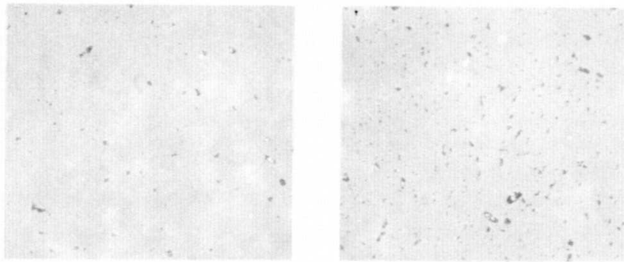

3.08 g/cc; A-6 mol% Y_2O_3-SiO_2 2.94 g/cc; B-3 mol% Y_2O_3-SiO_2

Figure 5. - Microstructures of β' - Si_3N_4 solid solution compositions sintered for 1 hour at 1700 C; X250.

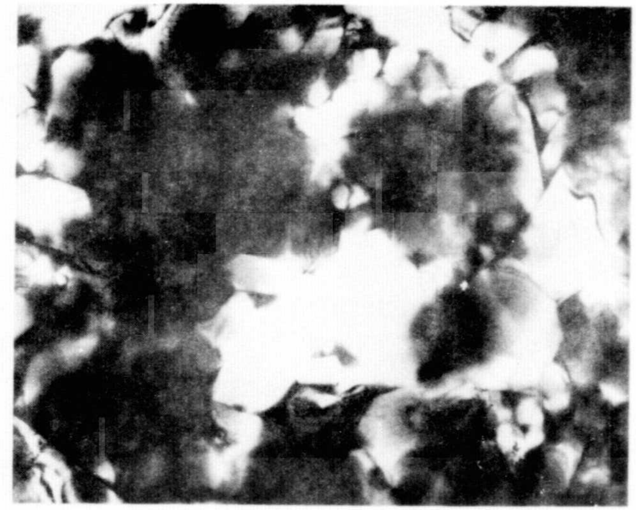

A-6 mol% Y_2O_3-SiO_2 1 μm Density - 3.08 g/cc

Figure 6. - Transmission electron micrograph of β'-Si_3N_4 solid solution showing both equiaxed and elongated grain structures.

ORIGINAL PAGE IS OF POOR QUALITY

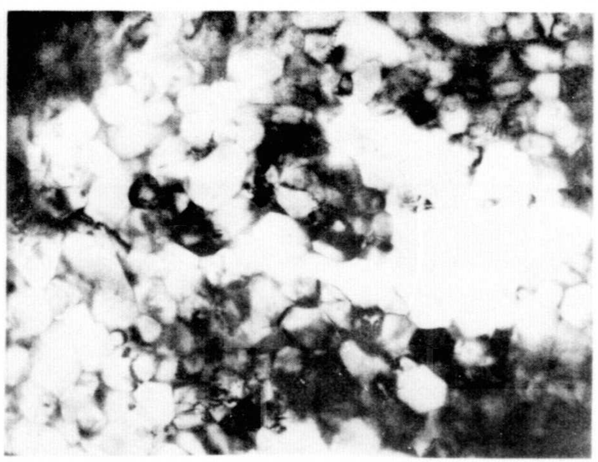

3 mol% Y_2O_3-SiO_2 1 μm Density - 2.94 g/cc

Figure 7. - Transmission electron micrograph of β' - Si_3N_4 solid solution showing faceted grain structures.

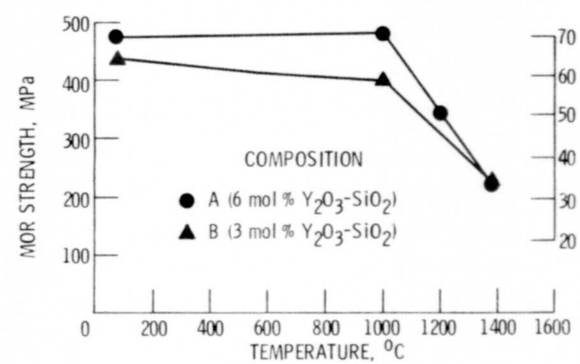

Figure 8. - Modulus of rupture strength (4-point bend) of β'-Si_3N_4 solid solutions.

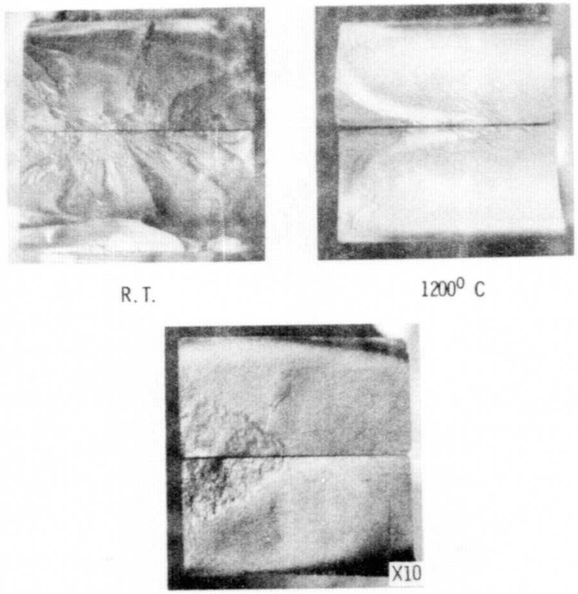

Figure 9. - Macrographs of β' - Si_3N_4 solid solution fractured at different temperatures; composition, A-6 mol% Y_2O_3-SiO_2; density, 3.08 g/cc.

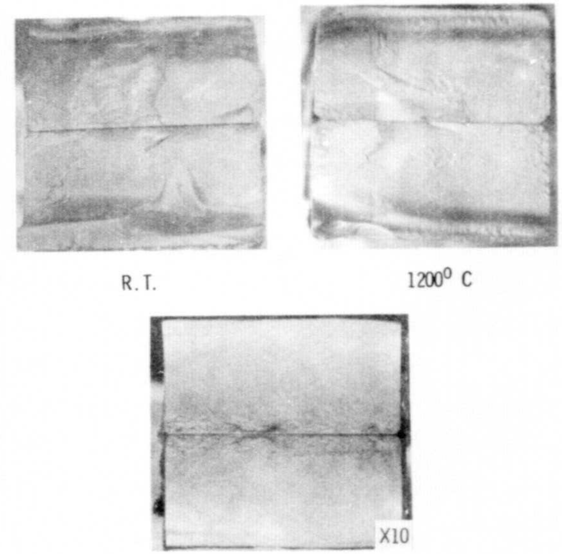

Figure 10. - Macrographs of β' - Si_3N_4 solid solution fractured at different temperatures; composition, B-3 mol% Y_2O_3-SiO_2; density, 2.94 g/cc.

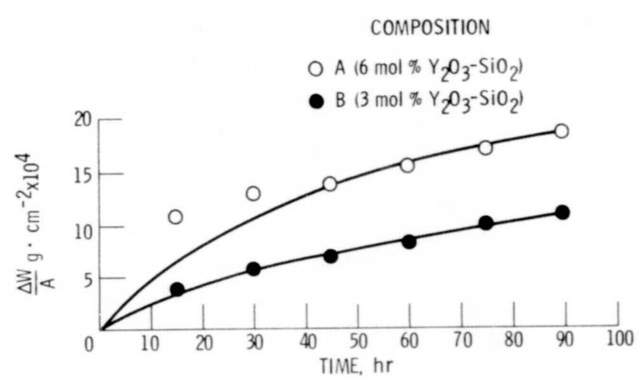

Figure 11. - Weight gain in air at 1375^0 C of β'-Si_3N_4 solid solutions (linear plot).

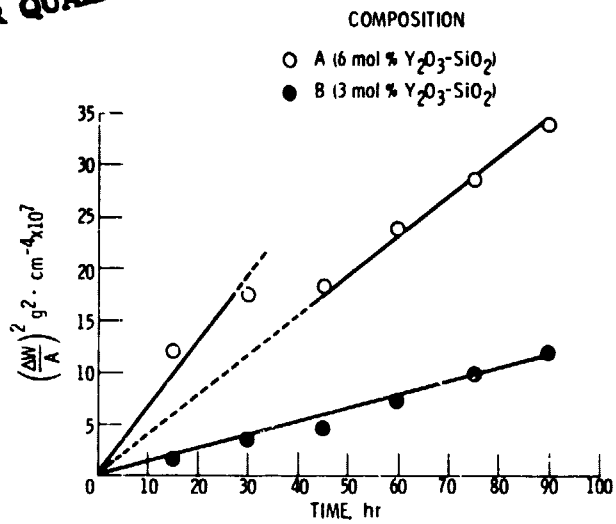

Figure 12. - Weight gain in air at 1375° C of β'-Si_3N_4 solid solutions (parabolic plot).

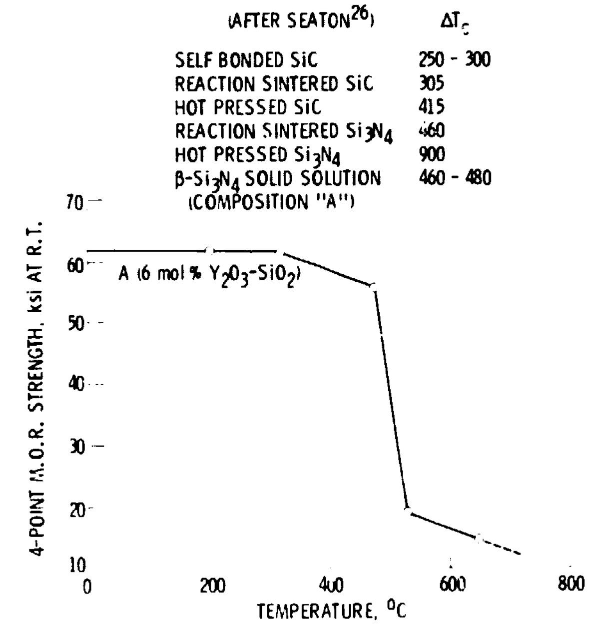

Figure 13. - Residual strength at room temperature after water quenching vs quench temperature for β'-Si_3N_4 solid solution (composition A).